A Simple Approach to Nonlinear Tensile Stiffness for Accurate Cloth Simulation

PASCAL VOLINO and NADIA MAGNENAT-THALMANN
MIRALab, University of Geneva
and
FRANCOIS FAURE
LJK, INRIA, University of Grenoble

Recent mechanical models for cloth simulation have evolved toward accurate representation of elastic stiffness based on continuum mechanics, converging to formulations that are largely analogous to fast finite element methods. In the context of tensile deformations, these formulations usually involve the linearization of tensors, so as to express linear elasticity in a simple way. However, this approach needs significant adaptations and approximations for dealing with the nonlinearities resulting from large cloth deformations. Toward our objective of accurately simulating the nonlinear properties of cloth, we show that this linearization can indeed be avoided and replaced by adapted strain-stress laws that precisely describe the nonlinear behavior of the material. This leads to highly streamlined computations that are particularly efficient for simulating the nonlinear anisotropic tensile elasticity of highly deformable surfaces. We demonstrate the efficiency of this method with examples related to accurate garment simulation from experimental tensile curves measured on actual materials.

1. INTRODUCTION

The mechanical properties of cloth materials are highly anisotropic and nonlinear: internal forces in the material are not at all proportional to the deformations, and they furthermore vary greatly with their orientation relative to the thread directions. This anisotropy and nonlinearity create significant challenges when it comes to defining a mechanical simulation system for accurately reproducing these effects on virtual objects for applications requiring accuracy, such as CAD systems. At the same time, interactive and virtual reality applications require very efficient simulation models capable of computing quickly enough in order to offer good reactivity to user interaction.

Our goal is to be able to accurately simulate complex cloth objects, such as complete garments on animated characters (Figure 1). Our contribution is to propose a new simulation model that accurately reproduces the nonlinear tensile behavior of cloth materials and which remains accurate and robust for very large deformations, while offering a very simple and streamlined computation process suitable for high-performance simulation systems. Unlike the majority of existing cloth simulation models, we intend to match as closely as possible, the actual behavior of cloth materials in large deformations using accurate strain-stress curves depicting the weft, warp, and shear tensile behavior traditionally considered in cloth characterization. Our model addresses elasticity as well as viscosity, making the model suitable not only for draping applications, but also for dynamic motion computations, which require mechanical damping. Finally we want to formulate this model as a simple and direct force computation over point masses associated with the vertices of an arbitrary triangle mesh. Hence, the model we propose is not much more complicated and time-consuming than the simple mass-spring models that are typically used in fast cloth simulation, while offering significantly more accuracy. Through this simple formulation, our model can be combined with the state of

Fig. 1.   The accurate simulation of complex garments requires mechanical models that precisely represent the nonlinear behavior of cloth materials.

the art numerical integration methods traditionally used with high-performance particle systems, along with collision techniques, also used in this context.

Our new computation scheme handles arbitrary triangle meshes, which are typically generated from Delaunay triangulation. The primary insight of our method is that there is no practical interest in linearizing expressions of a model intended to simulate essentially nonlinear behaviors. Therefore, we express strains and stresses in these elements according to the simple, however nonlinear Green-Lagrange tensor, as is similarly done for representing Saint-Venant-Kirchhoff materials. Our first contribution is to provide simple expressions relating material strain to particle positions, and material stress to particle forces, from which an accurate and efficient computation scheme can be obtained with simple and streamlined algorithms. Furthermore, we also relate material strain rate to particle velocities in the same manner, and this offers a new way of accurately representing material viscosity. Another contribution is to extend this representation through the use of nonlinear strain-stress relationships, which can be modeled so as to accurately represent the nonlinear behavior of cloth materials (Figure 2). Furthermore, these formulations allow the computation of a symmetric Jacobian of the elasticity forces without any approximations, offering high-performance simulation through efficient implicit integration methods or relaxation schemes that remain stable and robust even in the case of very large deformations. All these developments are expressed without excessively abstract formalisms in order to present a simple-to-implement view of our method.

The model we present only addresses tensile viscoelasticity, which deals with in-plane deformations. Meanwhile, bending elasticity deals with out-of-plane deformations (surface curvature), and its main visible effect is to limit fold curvature and wrinkle size. In the context of high-accuracy simulations, our tensile model can easily be complemented by a bending model using the schemes defined by Grinspun et al. [2003] or Volino and Magnenat-Thalmann [2006]. This is implemented in our system for producing the garments shown in Figure 1.

The remainder of this article is organized as follows. We first review key issues and previous work in Section 2.1, and describe the essential concepts of cloth viscoelasticity in Section 2.2. The computation scheme is then detailed in Sections 3.1 and 3.2 and summarized in Section 3.3. We demonstrate the accuracy and efficiency of this scheme in Section 4, and finally conclude in Section 5. The appendix explains how to accurately derive nonlinear strain-stress relationships from tensile tests in the context of large deformations.

2.   BACKGROUND

2.1   Mechanical Simulation Models

Early cloth simulation systems have been described as particle systems—systems where mass is concentrated at moving points called *particles*—and using forces directly derived from geometric criteria about the relative positions of the particles. They have long been of interest in the field of cloth simulation, and more generally in the field of interactive mechanical simulation, as they offer a simple, intuitive and flexible way to model mechanical systems. Furthermore, they can be used in conjunction with a large range of numerical integration schemes, according to the desired features of the simulation, for example, dynamic accuracy, convergence speed, fast and approximate simulation, robustness. . .

The first particle systems for cloth simulation were grid-based [Breen et al. 1994; Eberhardt et al. 1996], and already featured the simulation of nonlinear behavior curves through formulations that made them quite analogous to continuum mechanics models. Their accuracy was however fairly limited for large deformations and required quite long computation times. Faster models, based on mass-spring grids, have become popular since fast implicit numerical integration methods were used Baraff and Witkin [1998], because they allow a simple expression of the Jacobian of the particle forces while requiring only simple computations [Desbrun et al. 1999; Meyer et al. 2001; Choi and Ko, 2002]. Combined with advanced implicit integration methods [Eberhardt et al. 2000; Hauth and Etzmuss 2001; Volino and Magnenat-Thalmann 2005b], these simulation schemes have become popular for real-time and interactive applications. Unfortunately, mass-spring systems are unable to model surface elasticity accurately [Wang and Deravajan, 2005]. Although some techniques have been developed to match their parameters with those of the simulated material, they do not allow full discrimination among deformation modes [Bianchi et al. 2004], and they remain particularly inaccurate for anisotropic and nonlinear models. Such issues have given Particle Systems a reputation for inaccuracy.

On the other hand, finite elements have now acquired a good maturity for mechanical simulation. Their traditional field of application is elastic solid or shell modeling for mechanical engineering purposes, a context where linear elasticity and small deformations are the underlying assumptions. These formulations are not well adapted to very deformable objects such as cloth, and early attempts to model cloth using high-order elements [Eischen et al. 1996] led to impractically high computation times. However, it has been shown
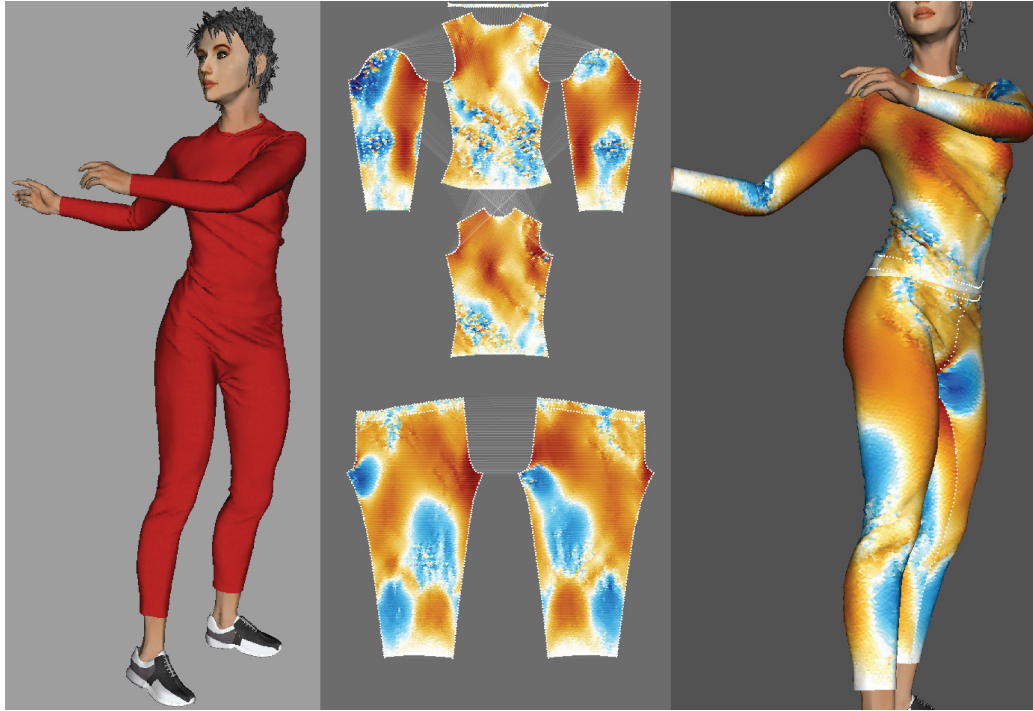
Fig. 2.   Accurate simulation of nonlinear anisotropic cloth materials is required for garment prototyping applications.

that the use of appropriate simplifications and efficient algorithms can make them usable in interactive graphics applications.

Finite element methods proceed in several steps. First, a deformation tensor is expressed at each point inside the elements, based on the shape functions associated with the nodes. When linear shape functions are used, the elements are called first degree, otherwise they are called higher degree. The computer graphics community has mainly considered first-degree elements, achieving a good compromise between speed and accuracy. Besides this, linearity can occur in two places in the finite element methods. The first, which we call geometrical linearity, is related to the way strains are computed from node displacements. A straightforward choice is to use Cauchy's strain tensor, which is linear with respect to node displacements, and leads to the fastest computations. However, large rotations generate well-known bulging artifacts. The most general way is to use Green-Lagrange's strain tensor, which is nonlinear with respect to node displacements and handles large rotations without artifacts. The other linearity, which we call material linearity, is related to the physical properties of the material. Most models consider the linear Hooke's law relating strain and stress.

Numerous authors have attempted to accelerate the computations required for finite elements. Pre-inverting the linear system matrix, as done by Desbrun et al. [1999] for particle systems, may speed up the computation [Bro-Nielsen and Cotin 1996; Cotin et al. 1999], but is only practical when the mechanical system is small enough. Condensing the dynamics on the boundary of a closed volume can reduce the number of unknowns to solve at each time step [James and Pai 1999]. These precomputations are possible when the force-displacement relation is linear, which requires both geometrical and material linearity.

Large rotations have been handled in two different ways. The most straightforward is to use Green-Lagrange's nonlinear strain measurement, while keeping material linearity. This is called the Saint-Venant-Kirchhoff model, mainly used in volume simulation [Bonet and Wood 1997; O'Brien and Hodgins 1999; Zhuang and Canny 2000; Debunne et al. 2001; Hauth et al. 2003; Picinbobo et al. 2003; Barbic and James 2005].

The force-displacement behavior of Saint-Venant-Kirchhoff models is less intuitive because of the nonlinearity of their strain and stress tensors. Hence, their strain is not proportional to the deformation of the material and the exerted force is not proportional to the stress. With strain-stress proportionality, the tensile force-deformation curve of such a material is cubic (Figure 3). However, their mathematical definition is the most mathematically natural way of expressing strain and stress, and indeed the simplest, despite the nonlinearity.

One drawback of this model is that it is not robust for soft materials under large compression, since it is prone to collapse [Bonet and Wood 1997, Figure 3]. Recently, a new approach has been proposed, where the strain tensor is factored as the product of a pure rotation with Cauchy's linear strain tensor aligned along the strain eigendirections [Muller et al. 2002; Hauth and Strasser 2004; Muller and Gross 2004; Irving et al. 2004; Nesme et al. 2005]. This corotational approach has become popular, as it combines the computational simplicity of using the linear Cauchy tensor with large deformations. This approach has been successfully used in cloth simulation [Etzmuss et al. 2003b], but material nonlinearity was not considered. The drawbacks of this method are mainly related to the additional computations required for managing these rotations.

Meanwhile, cloth materials are usually not subject to large compression, as their very low bending stiffness quickly allows them to buckle, relaxing compression to lower values. Hence, the compression collapse behavior of Saint-Venant-Kirchhoff models is not an issue in this context. It furthermore makes little sense to simulate
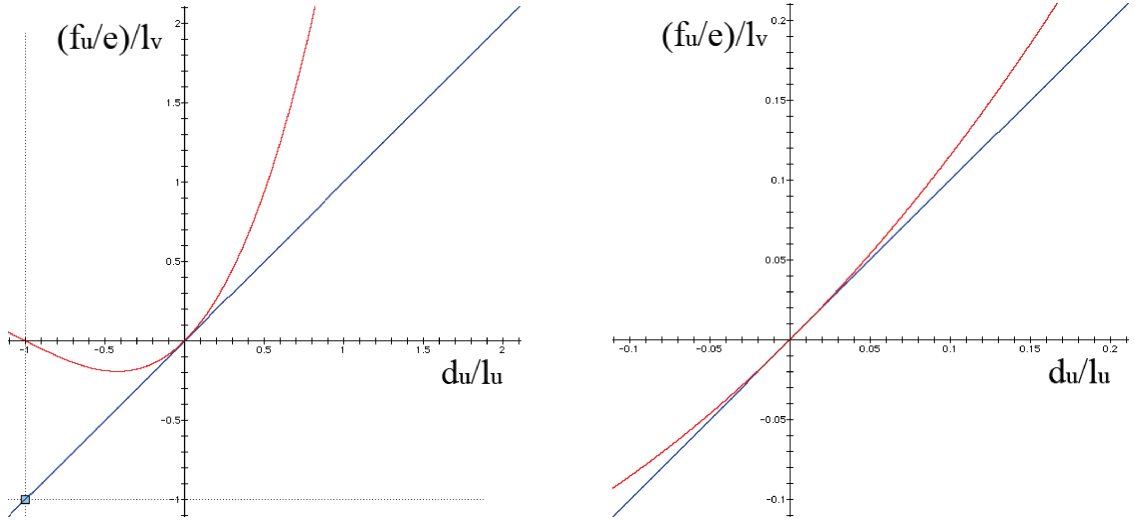
Fig. 3. Tensile elongation force-deformation curve of a St.Venant-Kirchhoff material (red) compared to a linear material (blue). Global view (left) and close-up (right). Notations correspond to the setup depicted in Figure 14. On the St.Venant-Kirchhoff material, we can note the collapse of the compression force for large compression deformation.

a perfectly linear force-deformation behavior for cloth materials, which are often highly nonlinear.

From this, we consider Saint-Venant-Kirchhoff models as being best suited to our purposes, namely for simulating anisotropic and nonlinear cloth materials under large deformations. They allow the computation to be kept as simple as possible, while being able to directly express the weft, warp, and shear stiffness, matching deformation modes used in traditional cloth characterization methods. Whereas the cubic tensile force-deformation behavior (Figure 3) is already a more realistic approximation of real cloth materials (Figure 7) than a linear force-deformation behavior when using proportional strain-stress laws. Our goal is to push accuracy a step further by extending the model to arbitrary nonlinear strain-stress laws, thereby allowing a very accurate fit to the actual nonlinear behavior of cloth material.

2.2 Tensile Viscoelasticity of Cloth

From the theory of elasticity [Timoshenko and Goodier 1970; Gould 1993], the internal tensile deformation of a surface is characterized by its strain, measured through a strain tensor, represented by three independent values $\varepsilon_{uu}, \varepsilon_{vv}$, and ε_{uv} related to the coordinate system (U, V) of the material. In dynamic systems, their rate is measured though their time derivatives $\varepsilon_{uu}', \varepsilon_{vv}'$, and ε_{uv}'. The internal tensile forces are characterized by its stress, modeled accordingly using a stress tensor represented by three independent values σ_{uu}, σ_{vv}, and σ_{uv}. The strain and stress values are related through the current energy per surface unit w of the material by the following relationships, for any deformation mode m among (uu, vv, uv):

$$\sigma_m = \frac{\partial w}{\partial \varepsilon_m}. \tag{1}$$

The relationship between strain and stress defines the mechanical behavior of the material. In the most general context, this is

expressed through the following strain-stress relationship:

$$
\begin{aligned}
&\sigma_{uu}\left(\varepsilon_{uu}, \varepsilon_{vv}, \varepsilon_{uv}, \varepsilon_{uu}', \varepsilon_{vv}', \varepsilon_{uv}'\right) \\
&\sigma_{vv}\left(\varepsilon_{uu}, \varepsilon_{vv}, \varepsilon_{uv}, \varepsilon_{uu}', \varepsilon_{vv}', \varepsilon_{uv}'\right) \\
&\sigma_{uv}\left(\varepsilon_{uu}, \varepsilon_{vv}, \varepsilon_{uv}, \varepsilon_{uu}', \varepsilon_{vv}', \varepsilon_{uv}'\right).
\end{aligned}
\tag{2}
$$

An *isotropic* material behaves identically irrespective of its orientation, and its strain-stress relationship does not depend on the orientation of the coordinate system associated to the material.

In the case of *linear viscoelasticity*, the strain-stress relationship can be expressed as a linear expression, the elastic and viscous stiffness of the material being represented as symmetric matrices E and E':

$$
\begin{bmatrix} \sigma_{uu} \\ \sigma_{vv} \\ \sigma_{uv} \end{bmatrix} = E \begin{bmatrix} \varepsilon_{uu} \\ \varepsilon_{vv} \\ \varepsilon_{uv} \end{bmatrix} + E' \begin{bmatrix} \varepsilon_{uu}' \\ \varepsilon_{vv}' \\ \varepsilon_{uv}' \end{bmatrix}. \tag{3}
$$

In the particular case of *isotropic linear elasticity*, the behavior of the material is only described with two parameters. Young's modulus, e, relates the stiffness of the material while the Poisson coefficient, ν, characterizes its transverse contraction upon extension (Figure 4). The corresponding matrix is given by:

$$
E = \frac{e}{1 - \nu^2} \begin{bmatrix} 1 & \nu & 0 \\ \nu & 1 & 0 \\ 0 & 0 & \frac{1-\nu}{2} \end{bmatrix}. \tag{4}
$$

While isotropic materials are well adapted for simulating homogeneous materials, cloth materials are mostly made of fibers that are oriented along particular directions. Thus they are very unlikely to exhibit the same stiffness in all directions. Therefore accurate representation of cloth materials requires anisotropic models (Figure 5). Among them, *orthotropic* models, which assume stiffness symmetry along orthogonal fiber directions (symmetric radial stiffness diagram as in Figure 5, far left), are only suitable for cloth having orthogonal fiber orientations with symmetric weave patterns.

Many simulation models exist for dealing with linear materials [Etzmuss et al. 2003a,b]. However, through the complexity of their
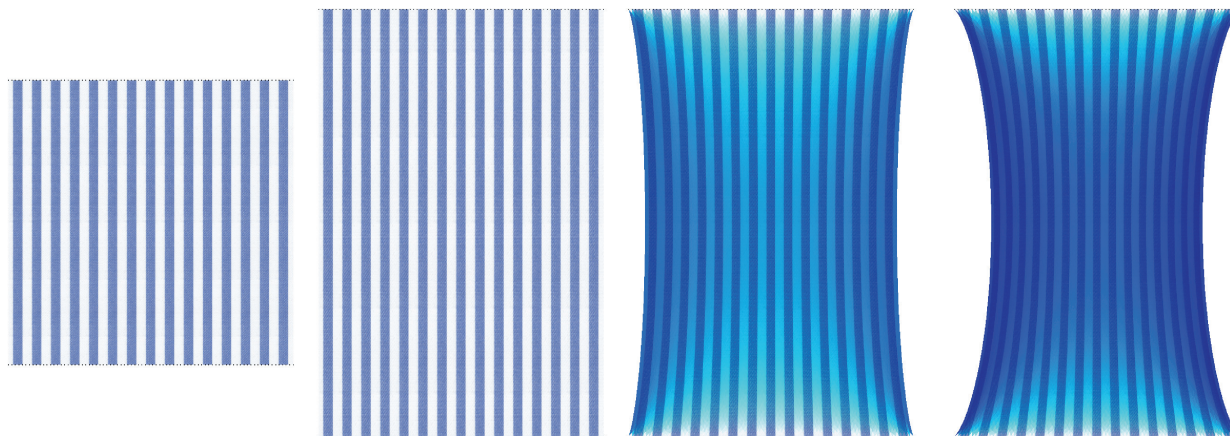
Fig. 4. A square piece of cloth attached at two opposite edges (far left), extended at 150% of its initial length. The material is linear isotropic, with a Poisson coefficient ν of 0 (left), 0.25 (center), 0.50 (right). Color is used to visualize the transverse compression strain.
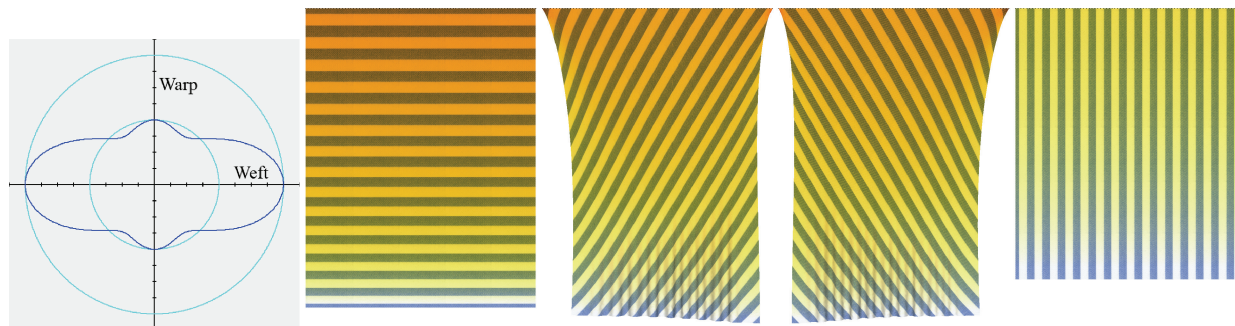

Fig. 5. A large square piece of cloth cut along various fiber directions, hanging attached at one edge (stripes are aligned to weft fiber direction). The material is linear anisotropic (3), with $2\,E_{uu,uu} = 1\,E_{vv,vv} = 8\,E_{uv,uv}$ (far left, radial elongation stiffness diagram depicting the elongation stiffness value relatively to the elongation orientation). This represents typical anisotropy of cloth materials, which usually have a much lower shear/elongation stiffness ratio than isotropic materials. Strips show weft fiber direction. Color is used to visualize the average tensile strain.
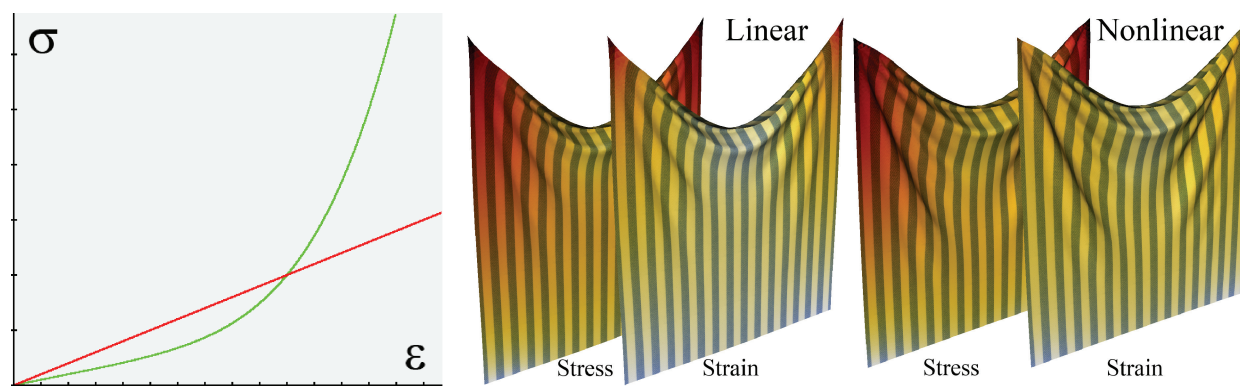
Fig. 6. A large square piece of cloth, hanging attached at two corners. The material is isotropic, with linear (left) (red curve far left) and nonlinear (right) (green curve far left) elongation strain-stress behavior. Color is used to visualize the average tensile stress (back) and strain (front). In both cases, there is a high concentration of stress around the attachment points that support the weight of the whole cloth. With a linear strain-stress behavior, this creates locally high strain, and therefore unrealistically large deformations in these areas. A nonlinear strain-stress behavior smoothes out the strain and the deformations are much more evenly distributed over the cloth.

Fig. 7. Weft (left) and warp (right) elongation tensile test of a cloth material with several load-unload cycles of various amplitudes. The precise evaluation of material plasticity requires a complex study of strain-stress hysteresis, far beyond the evaluation of the hysteresis envelope only.
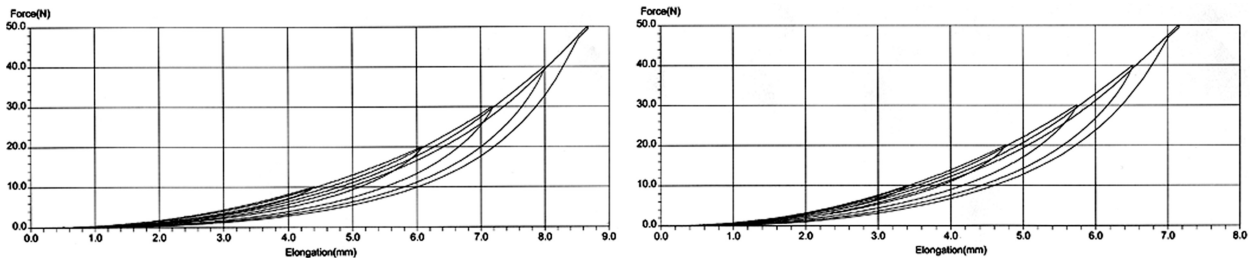
structure, cloth materials have very nonlinear behaviors. The internal deformations of the materials produce internal forces that are not proportional to the deformations. Linear strain-stress models are only a crude approximation of the actual behavior of cloth materials and they quickly show their limits for large deformations, as for instance the "superelasticity" artifact observed by Provot et al. [1995] (Figure 6). Therefore, accurate cloth simulation requires nonlinear models for closely fitting simulated cloth behavior to actual observed behavior, as measured through specific tensile tests (see Appendix). Our main interest is to address the case of nonlinear materials through their most general strain-stress behavior (2), which is needed for accurately representing the large-scale behavior of structures that have high small-scale complexity, such as cloth.

While elastic forces oppose deformation, viscous forces oppose deformation rate. Viscosity does not affect the rest geometry of the cloth in static contexts (draping), but it contributes to the damping of the cloth motion through energy dissipation.

In our model, through (2), viscosity is considered directly as a dependency of the stress to strain rate, rather than through a viscosity force opposing velocity, as in most existing models. This approach allows a mechanically-consistent representation of viscosity that may possibly be nonlinear, thereby allowing the modeling of complex dissipative effects. Because there is no practical procedure for measuring the actual tensile viscosity of cloth materials, viscous parameters are typically empirically determined in order to obtain realistic damping in the cloth motion.

Plasticity results from hysteresis in the strain-stress behavior of the material. It is quite significant for cloth materials, and it mainly results from the friction between the textile fibers. Like viscosity, the primary observable effect of plasticity is the damping of cloth motion caused by energy dissipation.

Our model can be extended to model plasticity through an adequate processing of the strain-stress behavior. The easiest solution, derived from Breen et al. [1994] is to modify the rest strain of the strain-stress laws according to the current strain-stress state of the system, simulating the solid friction between the fibers. More advanced models, which take into account time-dependent evolution of the rest strain, could take advantage of models based on Prony series approximations [Soussou et al. 1970], which can reproduce the quality factor of the hysteresis loops [Hauth et al. 2003]. However, a precise modeling of plasticity requires an accurate knowledge of the possibly time-dependent strain-stress behavior inside the hysteresis envelope, not only the envelope itself; this requires measuring the tensile properties of the cloth materials with more sophisticated procedures (Figure 7) than the single load-unload cycle usually performed. The complete study of plasticity and its simulation is a topic that is far beyond the scope of this work. Furthermore, the numerical simulation is itself quite unpractical and expensive due to the

numerical problems caused by the high nonlinearity of hysteresis. As a consequence, cloth simulation systems do not usually support accurate simulation of plasticity.

While unnecessary in the context of cloth draping applications, the accurate dynamic reproduction of cloth movement over time requires significant damping to avoid unrealistic underdamped oscillations. Whereas viscosity cannot be explicitly measured in cloth materials through simple and standard test procedures, it is nevertheless a simple solution for reproducing the global dissipative behavior caused by both plasticity and viscosity. In this context, some techniques attempt to identify viscous parameters of cloth materials by experimentally matching the simulated damping of its motion to actual samples [Bhat et al. 2003].

In the developments that follow, we formulate our model for general nonlinear anisotropic tensile viscoelasticity (2), which can also be extended for hysteresis formulations, as for example through Prony series. Adequate simplifications may then be carried out according to the actual simulation context.

3. THE SIMULATION SCHEME

Starting from the most general anisotropic nonlinear viscoelastic strain-stress relationship (2) describing the mechanical behavior of the material, we present a simple computation scheme that can be applied to meshes made of arbitrary triangle elements, such as those obtained through Delaunay triangulation of arbitrary surfaces. We consider these elements linear, having uniform geometrical and mechanical properties over the surfaces. Using the positions of mesh vertices as the only degrees of freedom, we describe a simple computation process to derive element strain from vertex positions and vertex forces from element stress (Section 3.1), as well as the corresponding Jacobian (Section 3.2).

3.1 Computing Forces

Our algorithm processes triangle elements of the mesh describing the surface (Figure 8 left). Each element is described by the 2D parametric coordinates $(u_a, v_a), (u_b, v_b), (u_c, v_c)$ of its vertices, referring to an orthonormal parametric coordinate system, which typically aligned with the weft and warp fiber directions. The current position of the deformed element is defined by the 3D world coordinates P_a, P_b, P_c of its vertices, and possibly velocity coordinates P'_a, P'_b, P'_c. The weft and warp vectors are expressed in 3D world coordinates as U and V, which are not necessarily orthonormal because of material deformation (Figure 8 right). In the following, these vectors will be used for measuring the deformation state of the element, as well as expressing any vector value related to the element in world coordinates.
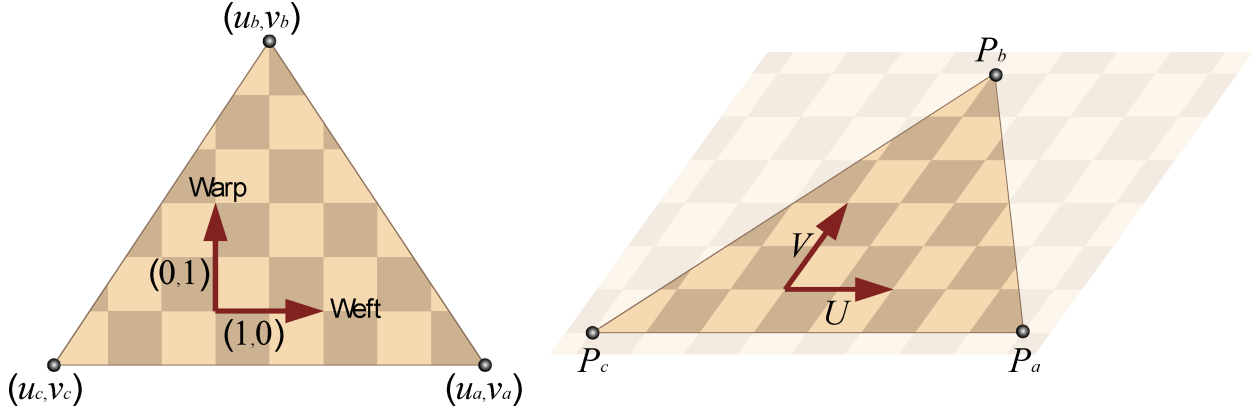
Fig. 8. A triangle element is defined in 2D parametric coordinates (left), and deformed in 3D world coordinates (right).

Our goal is to compute the deformation state of a triangle element directly from the positions of its vertices. To do this, we express the parametric coordinate basis vectors $(1,0)$ and $(0,1)$ as translation-independent weighted sums of the parametric coordinates of the three vertices (u_a,v_a), (u_b, v_b), (u_c,v_c) (Figure 8 left). This leads to the following linear systems:

$$\sum_i r_{ui}\ u_i = 1 \qquad \sum_i r_{vi}\ u_i = 0$$
$$\sum_i r_{ui}\ v_i = 0 \qquad \sum_i r_{vi}\ v_i = 1 \qquad (5)$$
$$\sum_i r_{ui} = 0 \qquad \sum_i r_{vi} = 0.$$

Solving these linear systems leads to the following weights, to be precomputed:

$$\begin{aligned} r_{ua} &= d^{-1}\ (v_b - v_c) & r_{va} &= d^{-1}\ (u_c - u_b) \\ r_{ub} &= d^{-1}\ (v_c - v_a) & r_{vb} &= d^{-1}\ (u_a - u_c) \\ r_{uc} &= d^{-1}\ (v_a - v_b) & r_{vc} &= d^{-1}\ (u_b - u_a). \end{aligned}$$
$$d = u_a\ (v_b - v_c) + u_b\ (v_c - v_a) + u_c\ (v_a - v_b) \qquad (6)$$

During the simulation, these values are the weights for computing the current 3D vectors U and V directly as a weighted sum of the current vertex positions P_i (Figure 8 right), as follows:

$$U = \sum_{i \in (a,b,c)} r_{ui}\ P_i \qquad V = \sum_{i \in (a,b,c)} r_{vi}\ P_i. \qquad (7)$$

When viscosity has to be considered in the context of dynamic simulations, the current evolution rates of the coordinate vectors U' and V' can be computed as well from the current vertex velocities P_i':

$$U' = \sum_{i \in (a,b,c)} r_{ui}\ P_i' \qquad V' = \sum_{i \in (a,b,c)} r_{vi}\ P_i'. \qquad (7')$$

Our model is based on the Green-Lagrange strain tensor, which allows the rotation-invariant description of internal surface strain in the context of large displacements. This symmetric tensor G is defined by the coordinate vectors as follows, I being the identity matrix representing the rest state:

$$G = \tfrac{1}{2}\ ([U\ V]^T\ [U\ V] - I). \qquad (8)$$

From this tensor, we can extract the weft warp and shear strain values, which respectively measure the elongation deformations along weft warp directions and the shear deformation between them, as

follows:

$$\begin{aligned} \varepsilon_{uu} &= \tfrac{1}{2}\ (U^T\ U - 1) \\ \varepsilon_{vv} &= \tfrac{1}{2}\ (V^T\ V - 1) \qquad (9) \\ \varepsilon_{uv} &= \tfrac{1}{2}\ (U^T\ V + V^T\ U). \end{aligned}$$

At this point, we can note that the strain is a quadratic expression of the vertex positions. We do not attempt to perform any linearization of these expressions.

Similarly, if viscosity is considered, the strain rate values are computed accordingly:

$$\begin{aligned} \varepsilon'_{uu} &= (U^T\ U') \\ \varepsilon'_{vv} &= (V^T\ V') \qquad (9') \\ \varepsilon'_{uv} &= (U^T\ V' + V^T\ U'). \end{aligned}$$

Having computed the strain state of the triangle surface, we can now obtain the stress state by using the strain-stress relationship (2), which characterizes the material of the surface.

The Green-Lagrange strain tensor is associated to the second Piola-Kirchhoff stress tensor through (1). The forces derive from energy [Bathe 1995]. Hence, the forces F_j exerted on the vertex j are computed by differentiation of the weft, warp, and shear components of the total elastic energy W of the triangle relative to the particle position P_j. Since we assume linear deformation of the triangle element, we have uniform strain, stress, and energy density w over its surface of area $\}d\ \}/2$ (6). Hence we have, for any j among (a,b,c):

$$F_j = -\frac{\partial W}{\partial P_j}^T = -\frac{|d|}{2}\ \frac{\partial w}{\partial P_j}^T = -\frac{|d|}{2}\left(\sum_{m \in (uu,vv,uv)} \sigma_m \left(\frac{\partial \varepsilon_m}{\partial P_j}^T\right)\right). \qquad (10)$$

With explicit expression of the derivatives of the Green-Lagrange strain values (9) using (7), we obtain:

$$F_j = -\frac{|d|}{2}\ (\sigma_{uu}\ (r_{uj}\ U) + \sigma_{vv}\ (r_{vj}\ V) + \sigma_{uv}(r_{uj}\ V + r_{vj}\ U)). \qquad (11)$$

Direct implementation of (7), (9), (2), and (11) can be the basis of an accurate simulator integrated using explicit numerical time-integration methods, such as Runge-Kutta [Eberhardt et al. 1996].

3.2 Computing the Jacobian

The Jacobian of the forces is necessary for implementing implicit numerical integration methods [Baraff and Witkin 1998; Eberhardt et al. 2000; Hauth et al. 2001; Volino and Etzmuss 2005], and any other relaxation schemes based on Newton iterations. Its accurate evaluation is necessary for good convergence and stability of state of the art simulation systems.

The elastic Jacobian contribution is computed from (10) and (2) as follows, for any i and j among (a,b,c):

$$\frac{\partial F_j}{\partial P_i} = -\frac{|d|}{2} \left(\sum_{\substack{m\in(uu,vv,uv)\\n\in(uu,vv,uv)}} \frac{\partial \sigma_m}{\partial \varepsilon_n} \left(\frac{\partial \varepsilon_m}{\partial P_j}^T \frac{\partial \varepsilon_n}{\partial P_i} \right) \right.$$
$$+ \sum_{\substack{m\in(uu,vv,uv)\\n\in(uu,vv,uv)}} \frac{\partial \sigma_m}{\partial \varepsilon'_n} \left(\frac{\partial \varepsilon_m}{\partial P_j}^T \frac{\partial \varepsilon'_n}{\partial P_i} \right)$$
$$\left. + \sum_{m\in(uu,vv,uv)} \sigma_m \left(\frac{\partial}{\partial P_i} \frac{\partial \varepsilon_m}{\partial P_j}^T \right) \right). \qquad (12)$$

A convenient and common approximation is to neglect the second term of this expression. Doing this, we neglect how strain rate depends on particle positions, and therefore how geometry variations affect viscous forces. This allows the complete decoupling between elasticity and viscosity components. This approximation does not affect the accuracy of the Jacobian of elastic forces in the context of very large deformations.

The viscous Jacobian contribution can be considered in the same manner, noting that the second and third terms are zero as strain values do not depend on particle velocities:

$$\frac{\partial F_j}{\partial P'_i} = -\frac{|d|}{2} \left(\sum_{\substack{m\in(uu,vv,uv)\\n\in(uu,vv,uv)}} \frac{\partial \sigma_m}{\partial \varepsilon'_n} \left(\frac{\partial \varepsilon_m}{\partial P_j}^T \frac{\partial \varepsilon'_n}{\partial P'_i} \right) \right.$$
$$+ \sum_{\substack{m\in(uu,vv,uv)\\n\in(uu,vv,uv)}} \frac{\partial \sigma_m}{\partial \varepsilon_n} \left(\frac{\partial \varepsilon_m}{\partial P_j}^T \frac{\partial \varepsilon_n}{\partial P'_i} \right)$$
$$\left. + \sum_{m\in(uu,vv,uv)} \sigma_m \left(\frac{\partial}{\partial P'_i} \frac{\partial \varepsilon_m}{\partial P_j}^T \right) \right). \qquad (12')$$

With explicit expression of the derivatives of the Green-Lagrange strain values (9) using (7), and with this approximation, we obtain the following. For simplicity, we write it here without the contributions of the cross-dependencies between the deformation modes:

$$\frac{\partial F_j}{\partial P_i} = -\frac{|d|}{2} \left(\begin{array}{l} \frac{\partial \sigma_{uu}}{\partial \varepsilon_{uu}} \left(r_{uj}\, r_{ui}\, U\, U^T \right) + \frac{\partial \sigma_{vv}}{\partial \varepsilon_{vv}} \left(r_{vj}\, r_{vi}\, V\, V^T \right) \\ + \frac{\partial \sigma_{uv}}{\partial \varepsilon_{uv}} \left(r_{uj}\, r_{vi} U\, V^T + r_{vj}\, r_{ui}\, V\, U^T \right) \\ + (\sigma_{uu}\, (r_{uj}\, r_{ui}) + \sigma_{vv}\, (r_{vj}\, r_{vi}) \\ + \sigma_{uv}\, (r_{uj}\, r_{vi} + r_{vj}\, r_{ui}))\, I \end{array} \right) \qquad (13)$$

and

$$\frac{\partial F_j}{\partial P'_i} = -\frac{|d|}{2} \left(\frac{\partial \sigma_{uu}}{\partial \varepsilon'_{uu}} \left(r_{uj}\, r_{ui}\, U\, U^T \right) + \frac{\partial \sigma_{vv}}{\partial \varepsilon'_{vv}} \left(r_{vj}\, r_{vi}\, V\, V^T \right) \right.$$
$$\left. + \frac{\partial \sigma_{uv}}{\partial \varepsilon'_{uv}} \left(r_{uj}\, r_{vi}\, U\, V^T + r_{vj}\, r_{ui}\, V\, U^T \right) \right). \qquad (13')$$

It can be noted that using this approximation, the elastic and the viscous Jacobian contributions are symmetric. This is an important feature for using the conjugate gradient method in the numerical solving scheme. They also have a regular structure, and the numerical solving scheme should take advantage of this for efficient numerical solving or sparse storage.

The expression of the elastic Jacobian contribution (13) has two components:

—a *stiffness component*, which depends on the strain-stress stiffness $\partial \boldsymbol{\sigma}/\partial \boldsymbol{\varepsilon}$;

—a *geometric component*, which depends on the stress value $\boldsymbol{\sigma}$.

Meanwhile, the expression of the viscous Jacobian contribution (13') has only a stiffness component.

The elastic and viscous stiffness terms $\partial \sigma/\partial \varepsilon$ and $\partial \sigma/\partial \varepsilon'$ are derived from (2). It can be noted that in the context of linear viscoelasticity (3), they are simply the elements of the stiffness matrices $\boldsymbol{E}$. and $\boldsymbol{E}'$.

The stiffness component represents how the strain-stress stiffness of the material acts in relationship to particle forces and positions. It is usually the most important component of the Jacobian. Meanwhile, the geometric component represents the particle force changes, which result solely from the evolution of the element geometry. For example, it represents the rotation of the particle forces as the element rotates. A linearized model based on the Cauchy tensor would not contain this geometric component.

In the context of small deformations, it often makes sense to ignore the geometric component of the Jacobian, assuming that the vectors $\boldsymbol{U}$ and $\boldsymbol{V}$ do not evolve far from their initial state. This is what happens when using the Cauchy linear approximation of the Green-Lagrange tensor, possibly addressing larger deformations through the corotational approach [Etzmuss et al. 2003b]. However, as pointed out by Choi and Ko [2002] in the context of mass-spring systems, the full evaluation of the Jacobian is important for the stability of the simulation of large deformations as encountered in cloth simulation, where elements may exhibit large orientation changes within few iterations. Fortunately, through the use of the simple, nonlinearized expression of the Green-Lagrange tensor, the expression of the geometric component is quite simple, and is furthermore isotropic, as it does not depend on the current values of $\boldsymbol{U}$ and $\boldsymbol{V}$. Therefore, this approach is the best for performing stable simulations of highly deformable nonlinear materials through the use of a Jacobian accurately matching the actual deformed state of the mechanical system, whatever the amount of deformation (Figure 9).

A potential problem related to this expression results from the possible negative eigenvalues that the isotropic Jacobian component might introduce in the linear system matrix of the integration scheme. While this is not a problem in the context of the accurate linear system-solving schemes used in most finite element models, it could potentially bring trouble if the conjugate gradient method is used, such as in most interactive simulation system-using implicit integration. There is little need to worry about the stiffness component, as positive eigenvalues are ensured by the physical plausibility of the material, given that forces usually monotonously oppose deformations. However, the geometric component is more likely to generate negative eigenvalues, particularly when the material compression state creates negative eigenvalues in the stress tensor. In the context of cloth simulation, this is not really an issue as surface buckling quickly absorbs large tensile compression. However, this still needs to be addressed for obtaining an always-stable simulation system, as highly compressed elements might always briefly occur during simulation. While filtering out negative eigenvalues from the global Jacobian is not a computationally practical option, a formal, fairly conservative solution would be to filter out the negative eigenvalues of the stress tensor through adequate projection
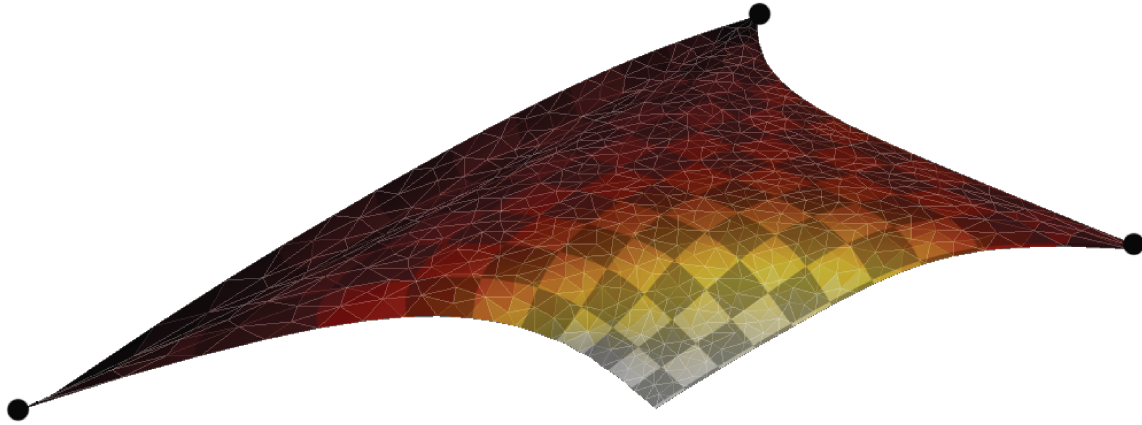
Fig. 9. An accurate Jacobian is necessary for stable simulation of very large deformations without compromising convergence speed. Color is used to visualize the mean strain value, here with a maximum of more than 400% elongation.

of the σ_{uu}, σ_{vv}, σ_{uv} values to be used in the computation of the geometric component. This is what Choi and Ko [2002] do with mass-spring systems. In practice, we find that a sufficient approximation for ensuring stability is to use null values of σ_{uu} or σ_{vv} if they are negative, thus avoiding any eigensystem computation.

3.3 Algorithm Summary

The computational process can be summarized in a ready-to-implement manner as follows.
Precomputation:

—For each element, evaluate and store the vertex distribution factors using (6).

Computation:

—For each element, evaluate the current material referential U and V from P_a, P_b, P_c using (7).
—Compute the strain values ε_{uu}, ε_{vv}, ε_{uv} using (9).
—Compute the stress values σ_{uu}, σ_{vv}, σ_{uv} using the mechanical behavior of the material (2).
—Compute the corresponding particle force contributions F_a, F_b, F_c using (11).
—If needed, compute the Jacobian contribution using (13) with the partial derivatives of (2).

3.4 Mass Lumping

A significant difference between finite elements and particle systems is that while the former accurately considers the mass of the mechanical system distributed over the surface of the elements, the latter concentrates the mass at discrete particle locations. Hence, the mass of a uniform triangle element is distributed equally on its three vertices. As a major benefit of this approximation, the inertia matrix only contains diagonal elements, and this simplifies the mechanical computations. This is why this approximation, known as *mass lumping*, is also often considered in usual finite element models.

In our model, mass lumping is implemented by assigning to each particle one third of the mass of all triangle elements adjacent to that particle in the mesh. The mass of an element is the mass per unit of area of the cloth material times the area, $|d|/2$, of the triangle. Through this, our model can be thought of as an efficient particle system.

4. PERFORMANCE

This model has been integrated in a cloth simulation system that allows interactive editing of cloth objects and collision processing for the creation and simulation of complete garments.

In our implementation, the mechanical model accepts independent weft, warp, and shear elastic strain-stress curves modeled as polynomial splines of any order. Possible cross-dependencies among these modes are also accepted by our system, for instance modeling transverse contraction. Viscosity is also modeled in the same way. External forces include gravity, anisotropic viscous aero-dynamic drag (wind), and collision effects (friction).

The resulting numerical system is integrated with backward Euler, implicit midpoint [Volino and Megnenat Thalmann 2005b] or alternatively BDF-2 [Hauth and Etzmuss 2001] numerical integration methods for performing dynamic cloth simulations. For cloth relaxation and draping applications, an iterative Newton resolution scheme is also implemented, which finds the particle positions that minimize the particle forces through the Jacobian. In any of these implicit schemes, our implementation uses, for each iteration, the Jacobian of the forces corresponding to the actual current state of the system. This variable Jacobian scheme, which accurately captures all the nonlinearities of the system, is made possible through on-the-fly evaluation of the Jacobian directly inside the numerical solving of the computation iteration, which is performed using the conjugate gradient method.

The computation code is written in standard C++ using double precision floating-point, and the tests are performed on a 3GHz Pentium4 PC.

4.1 Accuracy of the Model

Our accuracy test consists of simulating a virtual material described by its weft, warp, and shear nonlinear strain-stress curves, modeled from force-displacement curves of a tensile test. Through simulation, we perform a virtual tensile test of the material, comparing the resulting force-displacement curves to the experimental ones.

We performed this test using a 150 g/m^2 wool gabardine fabric, which is a fairly nonlinear material, highly anisotropic with weak shear stiffness.

We first measured the tensile weft, warp, and shear (along the weft) force-elongation curves using a tensile tester on the normalized 20 cm×5 cm sample. The averages of the load and unload
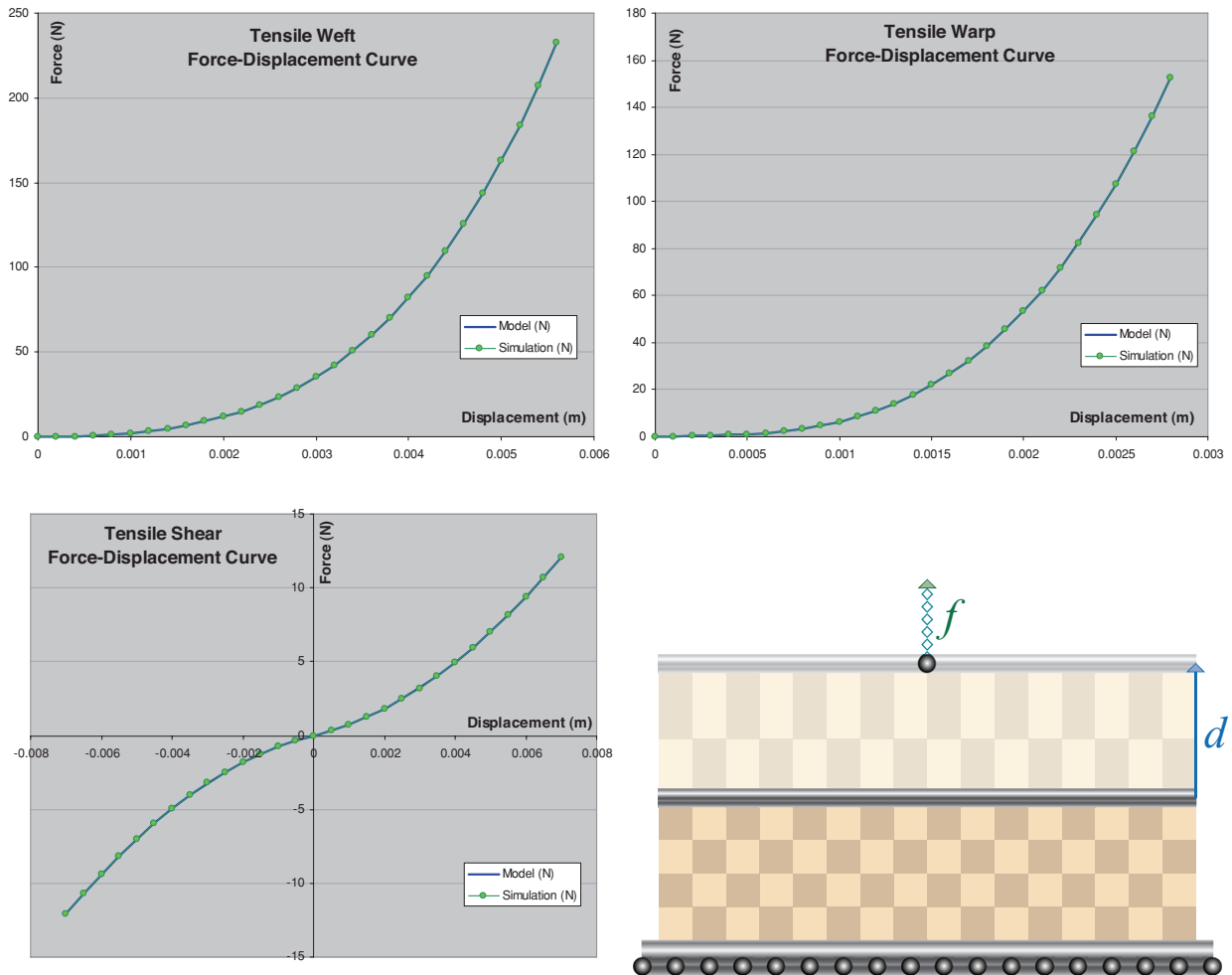
Fig. 10.   Comparing simulated weft, warp, and shear force-displacement curves with their counterparts defined in the model. With less than 0.01% difference, the curves are practically identical. The virtual tensile setup is shown at bottom right.

curves, once converted into strain-stress curves according to the formula given in the Appendix, are then modeled with polynomial splines using three segments, 3rd-order for elongation and 2nd-order for shear.

The virtual simulation of the experimental setup was then carried out on a sample of 2500 triangles: The cloth rectangle was attached along its two longest edges, and the total attachment force along one edge was measured according to its displacement. No other external force was considered and gravity was set to 0. Between each state change, the cloth equilibrium was computed using the Newton relaxation method.

The following force-displacement curves give the comparison between the polynomial model modeling the experimental data and the virtual test data. Note that the strain-stress curves are converted back to force-displacement curves (Figure 10).

From these curves, we can see that the force-displacement behavior produced by our simulation system precisely duplicates the force-displacement model resulting from the strain-stress polynomial spline model. The error remains below 0.01%, with force differences below 0.01 N whereas total forces may exceed 100 N.

This illustrates the high accuracy that our model can provide with nonlinear anisotropic materials undergoing large deformations. Such accuracy is expected, since our model accurately represents the mechanical constitutive laws of the material model through continuum mechanics without any approximation. Furthermore, since the computation of the Jacobian is also exact, the model converges in typically less than 10 iterations to reach the accuracy we attained, and is limited only by the numerical floating-point accuracy of the computations.

4.2 Real-World Accuracy

In order to verify the validity of our model for simulating cloth in a real-world situation, we conducted an experiment comparing the behavior of the real cloth with the simulated virtual cloth.

A piece of cloth was clamped horizontally on a circular frame (30 cm diameter), with as little initial tension as possible. A vertical force was exerted on a disk (6 cm diameter) placed in the middle of the cloth. The vertical displacement of the disk was measured as a function of the force (Figure 11). We chose a soft terry cloth, so as to observe large displacements that could be accurately measured.
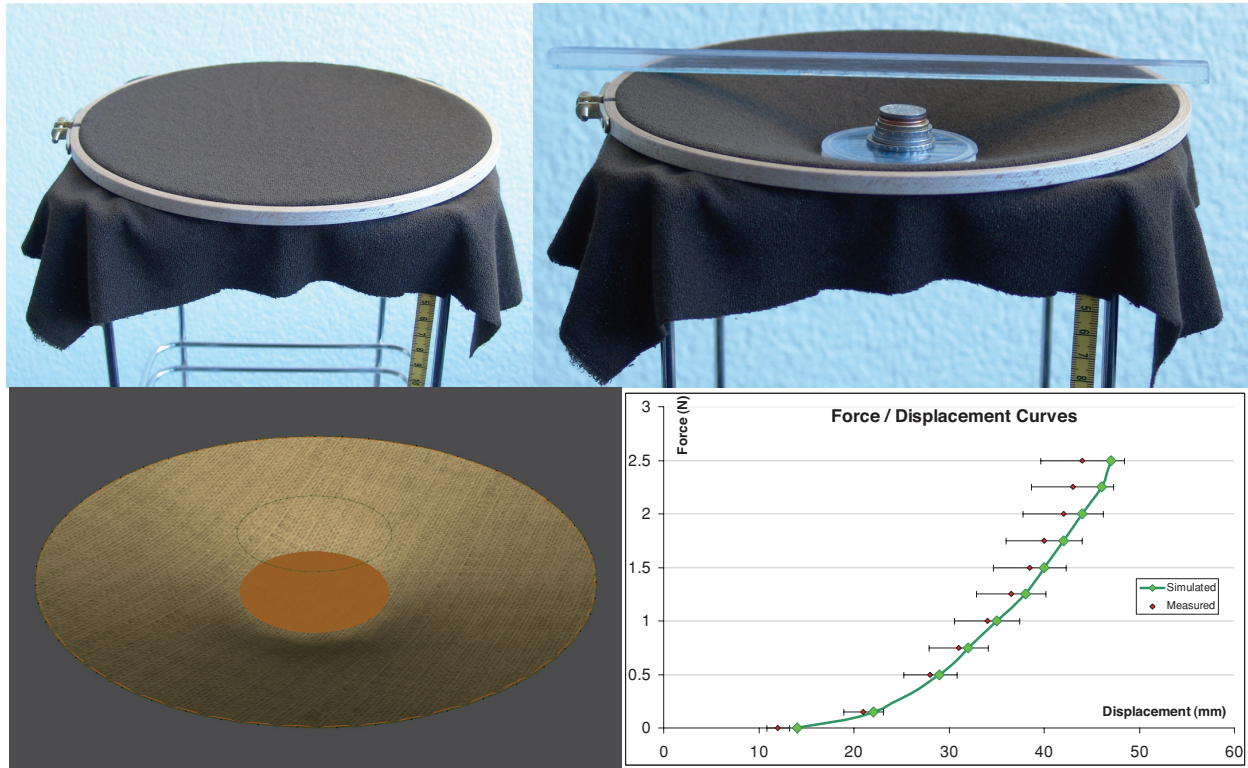
Fig. 11. The experimental setup (top), and the virtual simulation (bottom left). Depending on the force exerted by the weight on the middle of the cloth, the vertical displacement is plotted (bottom right), comparing the simulation (green curve) with the average of several experimental measurements (red dots with error bars showing average deviation).

For the results, we averaged several measurement sequences, which allows us to assess the accuracy of these measurements through the computation of the standard deviation. Observed measurement variations (around 10%) seem to result mainly from variations of the initial tension of the cloth on the frame, as well as possible plasticity effects of the material between each measurement. Strain-stress curves were accurately measured using tensile tests (as described in the Appendix), modeled as three independent (weft, warp, shear) polynomial splines (14) averaging the hysteresis loop, then used in our simulation system.

The measured curve (Figure 11 bottom right) shows that our simulation can reproduce the real cloth with good accuracy. In addition to the previously mentioned potential causes of error, the approximate modeling of the material could also be a source of error by not taking into account possible dependencies between weft, warp, and shear deformation modes, as discussed in the Appendix.

4.3 Computation Time

Computation times were measured on the dynamic simulation of a 1m×1m cloth square (Figure 12), initially horizontal, attached along one of its edges. Backward Euler integration was used for numerical integration, with constant simulation timesteps of 10 milliseconds.

For comparison purposes, we also implemented the linearized corotational scheme, obtained by rotation of the local element coordinates to the eigendirections of the strain tensor and linearization of the strain and stress expressions. It can be noted that the expression of the Jacobian is more complex because of the linearization, and requires approximations because of the state-dependent rotation.

We compared the computation time of our scheme and the linearized corotational scheme for computing 100 timesteps of the computation with several mesh resolutions. The material considered is a simple isotropic material (3), (4) of Young modulus $e = 1000$ N/m, and null Poisson coefficient $\nu = 0$. We also compared the computation time of a simple mass-spring system having springs defined along mesh edges modeling a similar elastic stiffness.

From the results, our implementation of the model is able to iterate more than 17,500 elements per second. The linearized corotational scheme is about two times slower. This slowdown does not only result from the computation of the eigensystem for evaluating the rotation, but also from the additional coordinate rotations, which account for a significant part of the total computation. This slowdown would be more significant if anisotropic materials were considered. Using a linearized scheme also requires additional vector normalizations (square roots), as well as a more complex, nonisotropic geometric component in the exact expression of the Jacobian (13). It should be noted that the numerical solving process, usually involving between 10 to 15 iterations of the conjugate gradient algorithm for each timestep, also accounts for more than half of the total computation time.

A simple mass-spring system is only marginally faster as compared to our scheme, with 20,000 elements iterated per second. Hence, our simulation scheme offers a significant increase in simulation accuracy for approximately 15% additional computation.
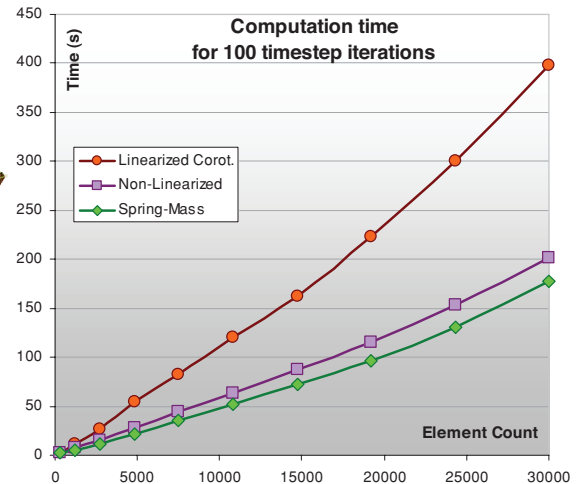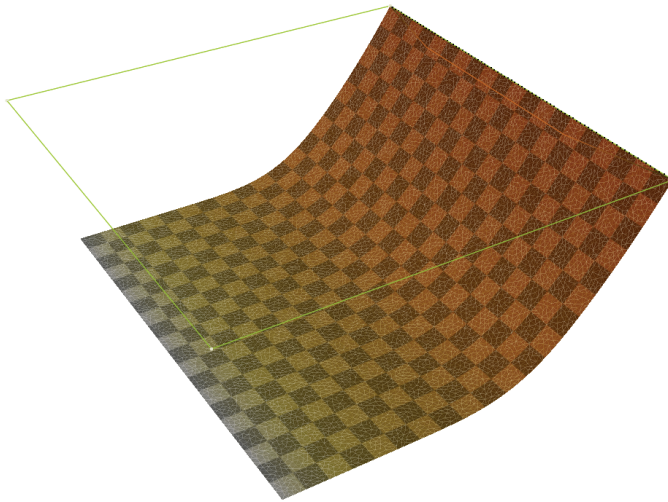
Fig. 12. Computation times required for the iterating the computation of 1m^2 of cloth, using various mesh resolutions, using our simulation scheme, the linearized corotational scheme, and a simple mass-spring scheme.

Tested under the same conditions as our simulation scheme, the nonlinear anisotropic strain-stress behavior defined in the previous section required roughly 10% additional computation.

4.4 Application: Virtual Prototyping

The proposed simulation technique has been implemented in a virtual prototyping system, which allows for the design of complex garments on mannequins. The efficiency of the model allows for the simulation of accurate mechanical properties of cloth materials on high-resolution meshes as the mannequin moves, allowing the garment designer to assess the stretch forces for particular postures (Figure 13). The design of the garment patterns may then be corrected accordingly, with interactive mechanical feedback on the garment drape. The proposed simulation technique allows complex multilayer garments to be simulated through an appropriate handling of complex collision situations. With the use of appropriate implicit integration methods, the model can efficiently compute both static drapes and dynamic animations.

5. CONCLUSION

We have presented a novel cloth simulation system based on continuum mechanics. Through the use of the non-linearized Green-Lagrange tensor, this model offers a simple and accurate way of modeling nonlinear anisotropic materials such as of cloth under large deformations, which can be obtained through the use of arbitrary strain-stress relationships.

The presented model offers considerable flexibility, and can be viewed as a particle system, through simple explicit relationships relating material strains and stresses to particle positions and forces. It avoids intermediate computations as much as possible, such as the coordinates transformations used in the corotational approach. Thanks to this simplicity, the Jacobian of the forces can be easily expressed without approximation, for use with any appropriate implicit numerical time integration method. This ensures not only good performance, but also robustness, providing numerically stable solutions even in the context of unrealistically large deformations.

The proposed simulation scheme is particularly well adapted for applications that need to combine good mechanical accuracy with computation times compatible with interactive applications. It is therefore a very good candidate for garment prototyping applications which require accurate representation of nonlinear anisotropic cloth material properties modeled from experimental data, thanks to the ability to use arbitrary nonlinear strain-stress relationships. If the computation was to be speeded up even more through the use of simple linear strain-stress relationships, the resulting St.Venant-Kirchhoff materials would still be better approximations of actual cloth material behavior than the linear behaviors frequently obtained in most existing fast simulation systems.

This highly streamlined computational process also opens the doors for parallelization and hardware implementation, which, through the rise of dedicated chips, represent the future of high-performance mechanical simulation.

Appendix: Tensile Tests for Measuring Strain-Stress Curves of Cloth

The tensile elastic behavior of cloth materials is usually characterized by its tensile elasticity strain-stress relationship, measured through adequate tensile tests. Standard procedures exist for characterizing cloth properties. For instance, the Kawabata evaluation system [Kawabata 1987] defines normalized hardware and tests for measuring weft warp elongation and shear strain-stress curves. It is important to note that the material is only considered through independent curves relating weft and warp elongation and shear, with no consideration of any possible cross-dependencies between deformation modes, and also with no consideration of the deformation rate (which is set to a single standard value). Then, the parameters of the cloth are evaluated as a set of characteristic values quantifying the shape of these curves. Since our concern is only related to the strain-stress curves of tensile elasticity, we can exploit weft warp elongation and shear curves measured by the Kawabata hardware (Figure 14 left), or use other tensile tests that may capture more complex behaviors in a wider range of deformations.

According to the Green-Lagrange tensor (8), The simplest and most natural way to integrate measured curves into our computation framework is to consider a simplified relationship between strain and stress (2) expressed as three decoupled (weft, warp, and shear)
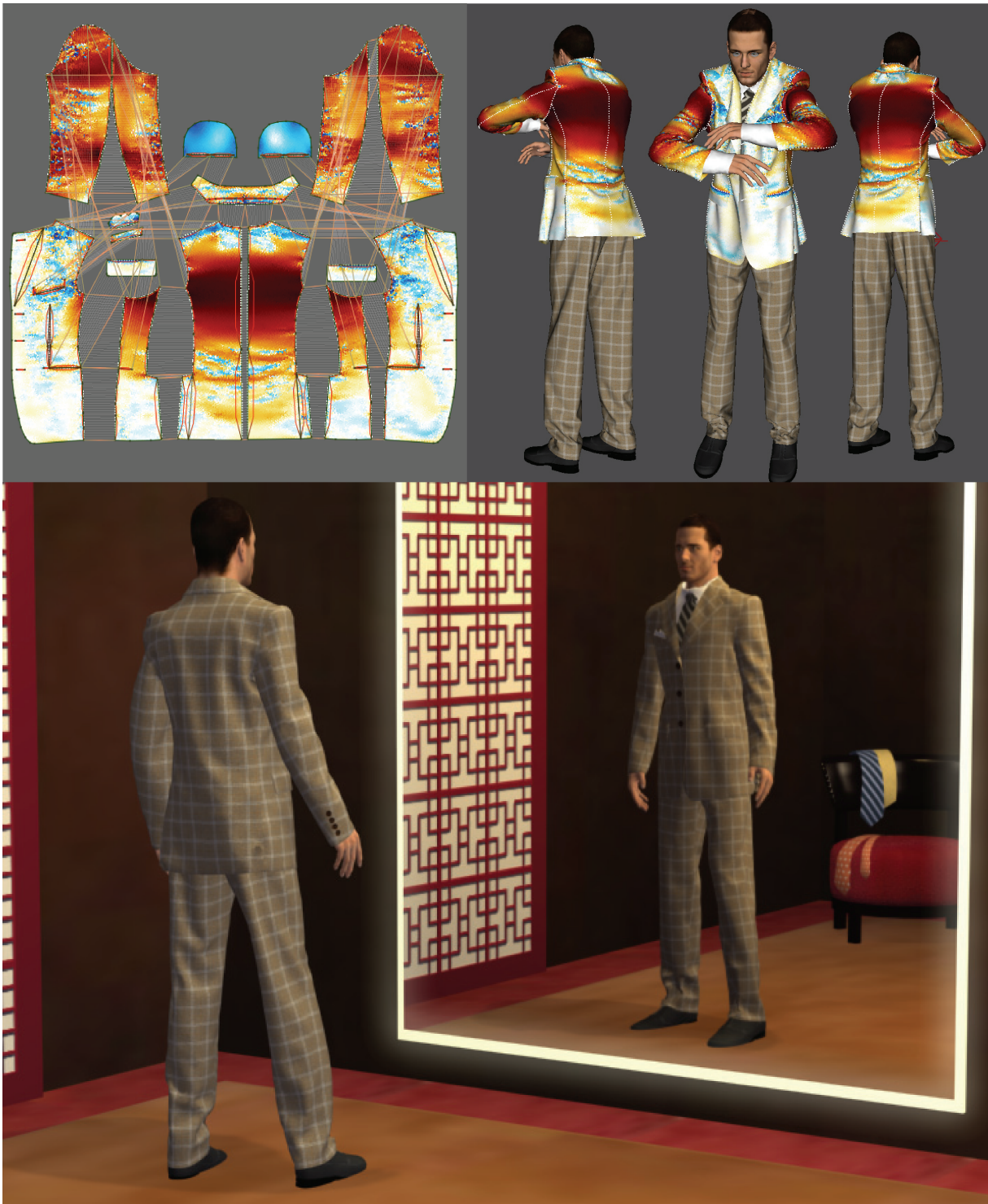
Fig. 13.   Virtual prototyping applications require an accurate representation of cloth material behavior for precisely evaluating the stretch forces (color scale) on the garment in particular postures of the character (top). In this example, the high-resolution jacket mesh is modeled using 8 mm triangles. Pattern resizing typically requires less than, one-minute computation for obtaining the corresponding drape. The computation of an animation typically requires between 5 to 20 minutes of computation per second of animation, collision processing accounting for the largest part of it.
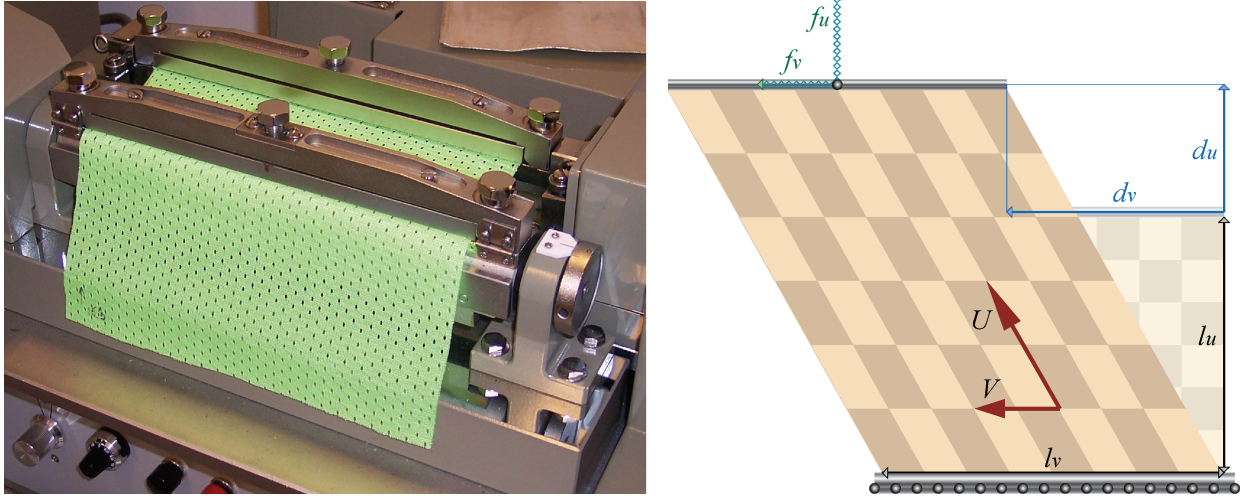
Fig. 14. Kawabata tensile tester (left): Notations for the elongation and shear tensile tests along the weft direction (right).
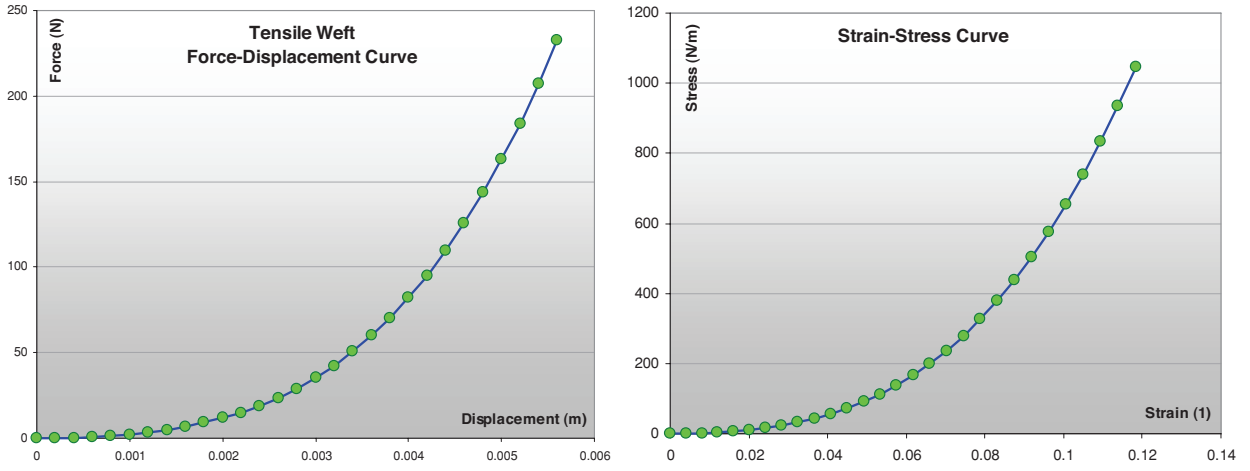

Fig. 15. Converting a tensile force-deformation curve (left) in into a strain-stress curve (right) using the Kawabata standard sample size ($l_u = 0.05$m, $l_v = 0.2$m).

curves, as follows:

$$\begin{aligned} \sigma_{uu}\,(\varepsilon_{uu}) \\ \sigma_{vv}\,(\varepsilon_{vv}) \\ \sigma_{uv}\,(\varepsilon_{uv}). \end{aligned} \tag{14}$$

However, through the nonlinearity of the Green-Lagrange tensor (8), the weft, warp, and shear strain and stress values cannot be directly identified to the measured force-deformation curves through a simple linear transformation. The purpose of this section is to establish the adequate conversion formulas (Figure 15), which should remain valid for large deformations.

For this, we consider a general tensile test (Figure 14 right), which combines elongation and shear deformation. Kawabata tensile measurements for elongation and shear are particular contexts of this general test. Hence, the sample size being l_u times l_v, a displacement of d_u elongation and d_v shear would produce a force of f_u elongation and f_v shear.

Through this deformation, the deformed weft and warp cloth coordinate vectors are expressed as follows:

$$U = \left(\frac{l_u + d_u}{l_u}, \frac{d_v}{l_u} \right) \quad V = (0, 1). \tag{15}$$

Using (9), we obtain the conversion formula from displacements to strain values:

$$\varepsilon_{uu} = \frac{d_u}{l_u} + \frac{d_u^2 + d_v^2}{2\,l_u^2} \quad \varepsilon_{uv} = \frac{d_v}{l_u}. \tag{16}$$

We also obtain the conversion formula from stress values to forces:

$$f_u = l_v\left(\sigma_{uu}\frac{l_u + d_u}{l_u} \right) \quad f_v = l_v\left(\sigma_{uv} + \sigma_{uu}\frac{d_v}{l_u} \right). \tag{17}$$

The forces are converted back to stress values as follows:

$$\sigma_{uu} = \frac{1}{l_v}\left(f_u\frac{l_u}{l_u + d_u} \right) \quad \sigma_{uv} = \frac{1}{l_v}\left(f_v - f_u\frac{d_v}{l_u + d_u} \right). \tag{18}$$

It can be noted that such tensile tests are unable to measure compression stiffness of cloth materials, since these buckle and exhibit wrinkle patterns upon compression because of their low bending stiffness. Nevertheless, cloth materials do have some compression stiffness, which is indeed necessary for their buckling behavior. Therefore, realistic cloth simulation requires compression stiffness to be modeled. High-accuracy models are however not required, since buckling allows relaxation and limits the actual cloth compression to low values. In practice, as compression stiffness is generally not measured, we typically extrapolate elongation strain-stress curves to negative values using antisymmetric functions.

It can also be noted that elongation and shear measurements can be carried out along both weft and warp directions (as done in the Kawabata standard), leading to a total of *four curves*. However, the mathematical definition of tensile deformation only allows its description as *three independent values*, that we have chosen in (14) to be weft, warp, and shear, as defined by the Green-Lagrange tensor (8) and (9). Assuming independence of the two elongation modes, the two shear force-deformation curves cannot be unrelated, and they should indeed produce identical shear strain-stress curves after conversion (this should also be true in any case in the context of linear elasticity). Therefore, a mismatch between them indicates that there is a significant nonlinear dependency between the deformation modes. In this case, accurate reproduction of the deformation behavior would require a more complex strain-stress relationship than only three independent curves.

More generally, some behaviors of the cloth material cannot be evaluated using curves from the Kawabata tests only. These include those resulting from the coupling of deformation modes, as for example transverse shrinking (which, in the context of linear elasticity (4), is represented by the Poisson coefficient (see Figure 4 in Section 2.1). Also, nonsymmetric cloth behaviors (possibly caused by nonsymmetric yarn patterns) need to be modeled with coupling between elongation and shear modes. It would be possible to evaluate with better accuracy the nonlinear strain-stress behavior of a cloth through more comprehensive force-deformation tests than what is proposed in the Kawabata standard, by simultaneously combining various values of elongation and shear deformations. Adequate interpolation functions would then model this data as a general strain-stress relationship (2) to be used as input in the proposed simulation scheme.

ACKNOWLEDGMENTS

REFERENCES

BARAFF, D. AND WITKIN, A. 1998. Large steps in cloth simulation, *Comput. Graph.* (*SIGGRAPH'98*), ACM Press, 43–54.

BARBIC, J. AND JAMES, D. L. 2005. Real-time subspace integration for St. Venant-Kirchhoff deformable models. In *Proceedings of the International Conference on Computer Graphics*.

BHAT, K. S., TWIGG, C. D., HODGINS, J. K., KHOSLA, P. K., POPOVIC, Z., AND SEITZ, S. M. 2003. Estimating cloth simulation parameters from video. In *Proceedings of SIGGRAPH-Eurographics Symposium on Computer Animation*. 37–51.

BATHE, K. J. 1995. *Finite Element Procedures*, Prentice Hall.

BIANCHI, G., SOLENTHALER, B., SZÉKELY, G., AND HARDERS, M. 2004. Simultaneous topology and stiffness identification for mass-spring models based on FEM reference deformations. In *Proceedings of the Medical Image Computing and Computer-Assisted Intervention*. C. Barillot, Ed. 2, 293–301.

BONET, J. AND WOOD, R. 1997. *Nonlinear Continuum Mechanics for Finite Element Analysis*. Cambridge University Press, Cambridge, UK.

BOURGUIGNON, D. AND CANI, M. P. 2000. Controlling anisotropy in mass-spring systems. In *Proceedings of the Eurographics Workshop on Computer Animation and Simulation*. 113–123.

BREEN, D. E., HOUSE, D. H., AND WOZNY, M. J. 1994. Predicting the drape of woven cloth using interacting particles. *Comput. Graph.* (*SIGGRAPH'94*), 365–372.

BRO-NIELSEN, M. AND COTIN, S. 1996. Real-time volumetric deformable models for surgery simulation using finite elements and condensation. In *Proceedings of the Eurographics*. ACM Press, 21–30.

CHOI, K. J. AND KO, H. S. 2002. Stable but responsive cloth. *Comput. Graph.* (*SIGGRAPH'02*), 604–611.

COTIN, S., DELINGETTE, H., AND AYACHE, N. 1999. Real-time elastic deformations of soft tissues for surgery simulation. *IEEE Trans. Visualization and Computer Graphics*, 5, 1, 62–73.

DESBRUN, M., SCHRÖDER, P., AND BARR, A. H. 1999. Interactive animation of structured deformable objects. In *Proceedings of Graphics Interface*. 1–8.

DEBUNNE, G., DESBRUN, M., CANI, M. P., AND BARR, A. H. 2001. Dynamic real-time deformations using space and time adaptive sampling. *Comput. Graph.* (*SIGGRAPH'01*). 31–36.

EBERHARDT, B., WEBER, A., AND STRASSER, W. 1996. A fast, flexible, particle-system model for cloth draping. In *IEEE Comput. Graph. Appl.* IEEE Press, 16, 5 52–59.

EBERHARDT, B., ETZMUSS, O., AND HAUTH, M. 2000. Implicit-explicit schemes for fast animation with particles systems. In *Proceedings of the Eurographics Workshop on Computer Animation and Simulation*. Springer-Verlag, 137–151.

EISCHEN, J. W., DENG, S., AND CLAPP, T. G. 1996. Finite element modeling and control of flexible fabric parts. *IEEE Comput. Graph. Appl.* IEEE Press, 16, 5, 71–80.

ETZMUSS, O., GROSS, J., AND STRASSER, W. 2003. Deriving a particle system from continuum mechanics for the animation of deformable objects. *IEEE Trans. Vis. Comput. Graph.* 9, 4, 538–550.

ETZMUSS, O., KECKEISEN, M., AND STRASSER, W. 2003. A fast finite element solution for cloth modeling. In *Proceedings of the 11th Pacific Conference on -Computer Graphics and Applications*, 244–251.

GOULD, P. 1993. *Introduction to Linear Elasticity*, 2nd edition. Springer.

GRINSPUN, E., HIRANI, A. H., DESBRUN, M., AND SCHRÖDER, P. 2003. Discrete shells. In *Proceedings of the Eurographics Symposium on Computer Animation*. 62–68.

HAUTH, M. AND ETZMUSS, O. 2001. A high performance solver for the animation of deformable objects using advanced numerical methods. In *Proceedings of Eurographics*. 137–151.

HAUTH, M., GROSS, J., AND STRASSER, W. 2003. Interactive physically-based solid dynamics. In *Proceedings of the Eurographics Symposium on Computer Animation*. 17–27.

HAUTH, M. AND STRASSER, W. 2004. Corotational simulation of deformable solids. In *Proceedings of the Winter School of Computer Graphics (WSCG)*. 137–145.

IRVING, G., TERAN, J., AND FEDKIW, R. 2004. Invertible finite elements for robust simulation of large deformation. In *Proceedings of the Eurographics Symposium on Computer Animation*. 131–140.

JAMES, D. AND PAI, D. 1999. ArtDefo–accurate real-time deformable objects. *Comput. Graph.* (*SIGGRAPH'99*), ACM Press, 65–72.

KAWABATA, S. 1987. *The Standardization and Analysis of Hand Evaluation*. The Textile Machinery Society, Osaka, Japan.

KEEVE, E., GIROD, S., PFEIFLE, P., AND GIROD, B. 1996. Anatomy-based facial tissue modeling using the finite element method. In *Proceedings of IEEE Visualization*. 21–30.

LLOYD, B., SZÉKELY, G., AND HARDERS, M. 2007. Identification of spring parameters for deformable object simulation. *IEEE Trans. Vis. Comput. Graph. 13*, 5, 1081–1094.

MEYER, M., DEBUNNE, G., DESBRUN, M., AND BARR, A. H. 2001. Interactive animation of cloth-like objects in virtual reality. *J. Vis. Comput. Anim. 12*, 1, 1–12.

MULLER, M. AND GROSS, M. 2004. Interactive virtual materials. In *Proceedings of Graphics Interface*. Canadian Human-Computer Communications Society, 239–246.

MULLER, M., DORSEY, J., MCMILLAN, L., JAGNOW, R., AND CUTLER, B. 2002. Stable real-time deformations. In *Proceedings of the Eurographics Symposium on Computer Animation*. 49–54.

NESME, M., PAYAN, Y., AND FAURE, F. 2005. Efficient, physically plausible finite elements. In *Proceedings of the Eurographics*. (short papers). 77–80.

PICINBONO, G., DELINGETTE, H., AND AYACHE, N. 2003. Nonlinear anisotropic elasticity for real-time surgery simulation. *Graph. Mod. 65*, 5, 305–321.

O'BRIEN, J. AND HODGINS, J. 1999. Graphical modeling and animation of brittle fracture. *Comput. Graph. (SIGGRAPH'99)*, ACM Press, 137–146.

PROVOT, X. 1995. Deformation constraints in a mass-spring model to describe rigid cloth behavior. In *Proceedings of Graphics Interface*. Canadian Human-Computer Communications Society, 147–154.

SOUSSOU, J. E., MOAVENZADEH, F., AND GRADOWCZYK, M. H. 1970. Application of prony series to linear viscoelasticity. *J. Rheol. 14*, 4, 573–584.

TESCHNER, M., HEIDELBERGER, B., MULLER, M., AND GROSS, M. 2004. A versatile and robust model for geometrically complex deformable solids. In *Proceedings of Computer Graphics International*.

TIMOSHENKO, S. P. AND GOODIER, J. N. 1970. *Theory of Elasticity*, 3rd Ed. McGraw-Hill.

VAN GELDER, A. 1998. Approximate simulation of elastic membranes by triangulated spring meshes. *J. Graph. Tools 3*, 2, 21–42.

VOLINO, P. AND MAGNENAT-THALMANN, N. 2005a. Accurate garment prototyping and simulation. *Comput.-Aid. Des. Appl. 2*, 5, 645–654.

VOLINO, P. AND MAGNENAT-THALMANN, N. 2005b. Implicit midpoint integration and adaptive damping for efficient cloth simulation. *Comput. Anim. Virt. Worlds 16*, 3–4, 163–175.

VOLINO, P. AND MAGNENAT-THALMANN, N. 2006. Simple linear bending stiffness in particle systems. In *Proceedings of the Eurographics Symposium on Computer Animation*. 101–105.

WANG, X. AND DEVARAJAN, V. 2005. 1D and 2D structured mass-spring models with preload. *Vis. Comput. 21*, 7, 429–448.

ZHUANG, Y. AND CANNY, J. 2000. Haptic interaction with global deformations. In *Proceedings of the IEEE International Conference on Robotics and Automation*.